Heteroatom-Doped Perihexacene from a Double Helicene Precursor: On-Surface Synthesis and Properties

Xiao-Ye Wang,[†] Thomas Dienel,[‡] Marco Di Giovannantonio,[‡] Gabriela Borin Barin,[‡] Neerav Kharche,[⊥] Okan Deniz,[‡] José I. Urgel,[‡] Roland Widmer,[‡] Samuel Stolz,[‡] Luis Henrique De Lima,[⊗] Matthias Muntwiler,[⊗] Matteo Tommasini,[#] Vincent Meunier,[⊥] Pascal Ruffieux,[‡] Xinliang Feng,[∥] Roman Fasel,*[,‡,∇] Klaus Müllen,*[,†] Akimitsu Narita*[,†]

[†]Max Planck Institute for Polymer Research, Ackermannweg 10, 55128 Mainz, Germany

[‡]Empa, Swiss Federal Laboratories for Materials Science and Technology, 8600 Dübendorf, Switzerland

[⊥]Department of Physics, Rensselaer Polytechnic Institute, Troy, 12180 New York, USA

[⊗]Paul Scherrer Institut, 5232 Villigen PSI, Switzerland

[#]Dipartimento di Chimica, Materiali ed Ingegneria Chimica 'G. Natta', Politecnico di Milano, Piazza Leonardo da Vinci 32, 20133 Milano, Italy

[∥]Center for Advancing Electronics Dresden, Department of Chemistry and Food Chemistry, Technische Universität Dresden, 01062 Dresden, Germany

[∇]Department of Chemistry and Biochemistry, University of Bern, 3012 Bern, Switzerland

1. General Method

All commercially available chemicals were used without further purification unless otherwise noted. Column chromatography was done with silica gel (particle size 0.063-0.200 mm) and thin layer chromatography (TLC) was performed on silica gel-coated aluminum sheets with F254 indicator. All yields given refer to isolated yields. Nuclear magnetic resonance (NMR) spectra were recorded on an AVANCE 300 MHz Bruker spectrometer. Chemical shifts were reported in ppm. Coupling constants (J values) were reported in Hertz. ^{1}H NMR chemical shifts were referenced to $CHDCl_2$ (5.320 ppm) or C_2HDCl_4 (6.000 ppm). ^{13}C NMR chemical shifts were referenced to CD_2Cl_2 (54.00 ppm). The attached proton test (APT) technique of ^{13}C NMR (J-modulated spin-echo for ^{13}C-nuclei coupled to ^{1}H-nuclei) was used to distinguish the carbon atoms with even or odd number of attached protons. The quaternary (C) and methylene (CH_2) signals were in the upper phase and the methine (CH) and methyl (CH_3) signals were in the opposite phase. Field desorption mass spectrometry (FD-MS) was carried out on a VG-Instrument ZAB 2-SE-FDP. High-resolution mass spectrometry (HRMS) was performed either on a Q-Tof Ultima 3 (micromass/Waters) by electrospray ionization (ESI) or on a SYNAPT G2 Si high resolution time-of-flight mass spectrometer (Waters Corp., Manchester, UK) by matrix-assisted laser desorption/ionization (MALDI) with tetracyanoquinodimethane (TCNQ) as the matrix. Absorption spectra were recorded on a Perkin-Elmer Lambda 900 spectrophotometer. Photoluminescence spectra were recorded on a J&MTIDAS spectrofluorometer. The photoluminescence quantum yield (Φ_F) was measured with 9,10-diphenylanthracene as a standard.[1]

All surface-assisted experiments were performed in ultrahigh vacuum (UHV) chambers with a base pressure of 10^{-11} mbar. The Au(111) single crystal was cleaned by sputtering (Ar$^+$, 1 keV) and annealing up to 750 K. The precursor **2** was thermally evaporated onto the Au(111) surface held at room temperature. The sublimation temperature of precursor **2** is 635 K.

Scanning tunneling microscopy (STM) and atomic force microscopy (AFM) experiments were carried out with a low-temperature scanning probe microscopy

system (LT-SPM, ScientaOmicron, Germany) at a temperature of 4.9 K. Scanning tunneling spectra (dI/dV) were detected with a lock-in amplifier (HF2LI by Zurich Instruments, Switzerland). Commercial Qplus sensors[2] equipped with tungsten tips (resonance frequency = 22350 Hz, Q-factor = 11000; tunneling current separated, ScientaOmicron) were used for non-contact AFM (nc-AFM) measurements. Repeated indentation to the substrate was used to shape the apex of the tip prior to the pick-up of a CO molecule from the sample.[3] Frequency-shift images at constant height with the CO-sensitized tip were performed with an amplitude of 100 pm.

X-ray photoelectron spectroscopy (XPS) measurements were performed on the PEARL beamline of the SLS synchrotron radiation facility (Villigen, Switzerland), using linearly polarized radiation with photon energy of 425 eV.[4] After deposition at room temperature, the sample was then transferred into the analysis chamber where the fast-XPS map was recorded during the in-situ annealing of the sample. High-resolution XPS (HR-XPS) spectra were recorded before and after the temperature ramp. XPS spectra were obtained in normal emission geometry, using a hemispherical electron analyzer equipped with a multichannel plate (MCP) detector. HR-XPS spectra were recorded in "sweep" mode with 20 eV pass energy, while the fast-XPS measurement was performed using the "fix" mode (snapshots of the C 1s level) acquiring one spectrum every 5 s with 50 eV pass energy.

Raman spectroscopy was performed in a Bruker Senterra Raman Microscope using a 532 nm laser (corresponding to 2.33 eV excitation energy). The Raman spectra of the perihexacene analogue **1** were acquired using three scans of 60 seconds adopting 2 mW laser irradiation power; the Raman spectra of the precursor **2** were acquired using a single scan of 10 seconds adopting 0.2 mW laser irradiation power. In both cases a 50× objective lens was used, which results in a 1-2 μm spot size. The Raman spectrum of **1** was measured on the Au(111) surface, while the Raman spectrum of **2** was measured on the powder sample.

2. Procedures of Solution Synthesis

3   1) *n*-BuLi, THF   2) Br⌒Br   **4**
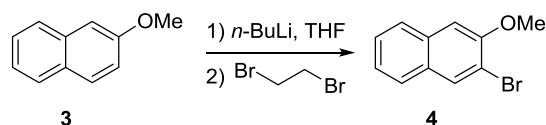
2-Bromo-3-methoxynaphthalene (4).[5] To a solution of 2-methoxynaphthalene (15.8 g, 100 mmol) in dry THF (120 mL) was added *n*-BuLi (1.60 M in hexane, 66.0 mL, 106 mmol) at −78 °C under argon. After the mixture was stirred at room temperature for 1 h, 1,2-dibromoethane (20.7 g, 110 mmol) was added at −78 °C. The resulting mixture was then stirred at room temperature for 24 h before quenching by an aqueous NH_4Cl solution. The mixture was extracted with ether (30 mL × 3) and the combined organic layers were washed with brine and water and dried over $MgSO_4$. After removal of the solvent under reduced pressure, the residue was purified by recrystallization from hexane to give 17.5 g of compound **4** (74%) as a white solid. ^{1}H NMR (300 MHz, CD_2Cl_2, 298 K, ppm) δ 8.07 (s, 1H), 7.75 (dd, J = 8.3, 1.4 Hz, 1H), 7.71 (dd, J = 8.1, 1.4 Hz, 1H), 7.47 (ddd, J = 8.3, 6.9, 1.4 Hz, 1H), 7.37 (ddd, J = 8.1, 6.9, 1.4 Hz, 1H), 7.20 (s, 1H), 3.99 (s, 3H). ^{13}C NMR (75 MHz, CD_2Cl_2, 298 K, ppm) δ 154.16, 134.20, 132.74, 129.96, 127.30, 127.21, 127.14, 125.04, 113.82, 107.27, 56.76. FD-MS (8 kV) m/z: Calcd for $C_{11}H_9BrO$: 236.0; Found: 235.9 (100%) [M][+].

4   1) Mg, THF   2) hexabromobenzene   3) I_2 **5**
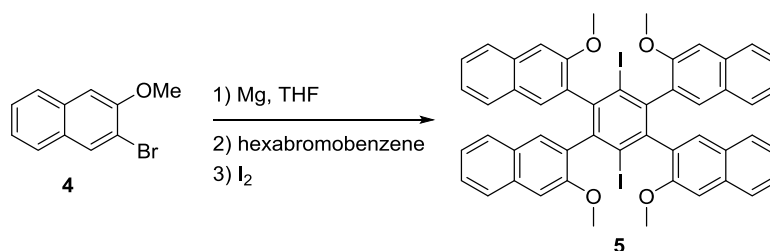
1,4-Diiodo-2,3,5,6-tetra(3-methoxynaphthalen-2-yl)benzene (5). To a Schlenk flask containing activated Mg (480 mg, 20.0 mmol) and 5 mL of dry THF was slowly added a solution of 2-bromo-3-methoxynaphthalene (**4**) (3.79 g, 16.0 mmol) in 20 mL of dry THF. After the mixture was stirred at 60 °C for 2 h, the generated Grignard reagent was transferred into a Schlenk tube charged with hexabromobenzene (1.10 g,

2.00 mmol) under argon and the resulting mixture was stirred at 80 °C for 24 h. Iodine (3.05 g, 12.0 mmol) was added at 0 °C and the reaction mixture was stirred at room temperature for 2 h. After quenching with water, the mixture was extracted with chloroform for three times. The combined organic layers were washed with brine and water and dried over $MgSO_4$. After removal of the solvents under reduced pressure, the residue was purified by column chromatography over silica gel (eluent: hexane/CH_2Cl_2 = 1 : 1), and then sonicated in 3 mL of toluene, filtrated, and washed with hexane to give 496 mg (26%) of compound **5** as a white solid. ^{1}H NMR (300 MHz, $C_2D_2Cl_4$, 298 K, ppm) δ 8.04 − 6.25 (m, 24H, aromatic signals of stereoisomers), 4.20 − 3.45 (m, 12H, methyl signals of stereoisomers). HRMS (ESI) *m/z*: Calcd for $C_{50}H_{37}O_4I_2$: 955.0781; Found: 955.0767 [M + H]$^+$.
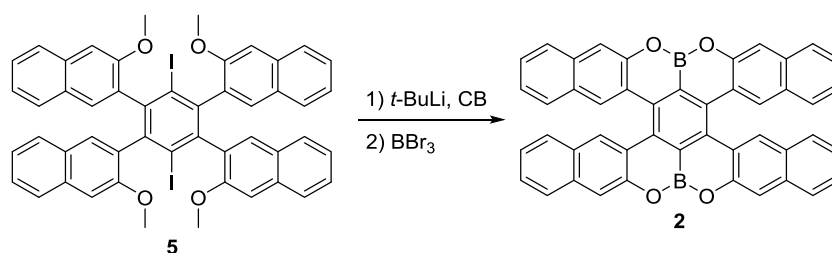
12a,26a-Dibora-12,13,26,27-tetraoxa-benzo[1,2,3-*hi*:4,5,6-*h'i'*]dihexacene (2). To a solution of compound **5** (0.14 g, 0.15 mmol) in anhydrous chlorobenzene (10 mL) was added *t*-BuLi (1.7 M in hexane, 0.35 mL, 0.60 mmol) at −45 °C under argon. After stirring at 0 °C for 3 h, BBr$_3$ (1.0 M in heptane, 0.40 mL, 0.40 mmol) was added at −45 °C. The reaction mixture was stirred at 40 °C for 24 h. After quenching with methanol, the precipitate was filtrated and washed thoroughly with methanol, water, acetone, dichloromethane, and hexane, to afford 43 mg (43%) of compound **2** as a yellow solid. The solubility of **2** in CD_2Cl_2, $CDCl_3$, 1,1,2,2,-tetrachloroethane-d_4, toluene-d_8, DMSO-d_6, etc. was extremely low, so that even an ^{1}H NMR spectrum could not be recorded at high temperatures (up to 140 °C). HRMS (MALDI) *m/z*: Calcd for $C_{46}H_{24}B_2O_4$: 662.1861; Found: 662.1876 [M]$^+$.
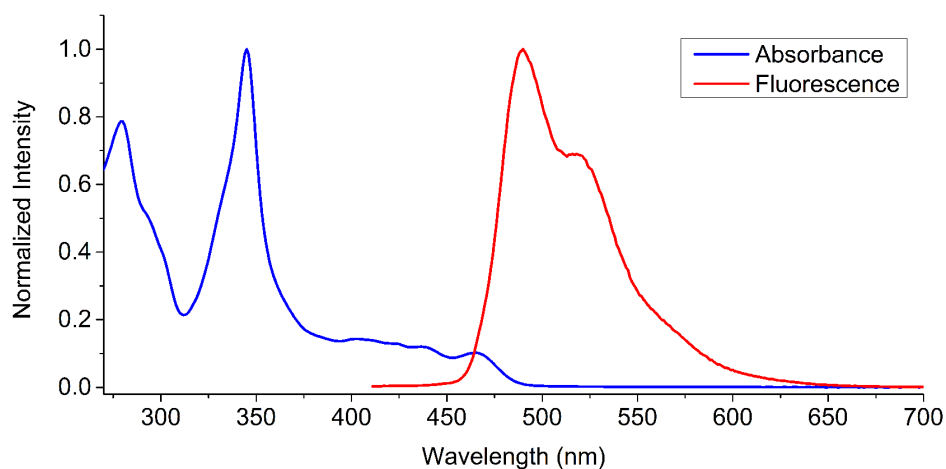
3. Photophysical Properties

Figure S1. Absorption and emission spectra of **2** in $C_2H_2Cl_4$ solutions. The absorption maximum is at 345 nm (absorption coefficient: 6.9×10^4 M^{-1} cm^{-1}). The absorption onset is at 487 nm, corresponding to an optical energy gap of 2.55 eV. According to time-dependent density functional theory (TD-DFT) calculations, the lowest energy absorption is assigned to the HOMO→LUMO transition, whereas the absorption maximum is mainly contributed to by the HOMO−5→LUMO transition (Figure S7). A green-yellow fluorescence was observed for compound **2**, with an emission maximum at 490 nm and a quantum yield (Φ_F) of 3%.
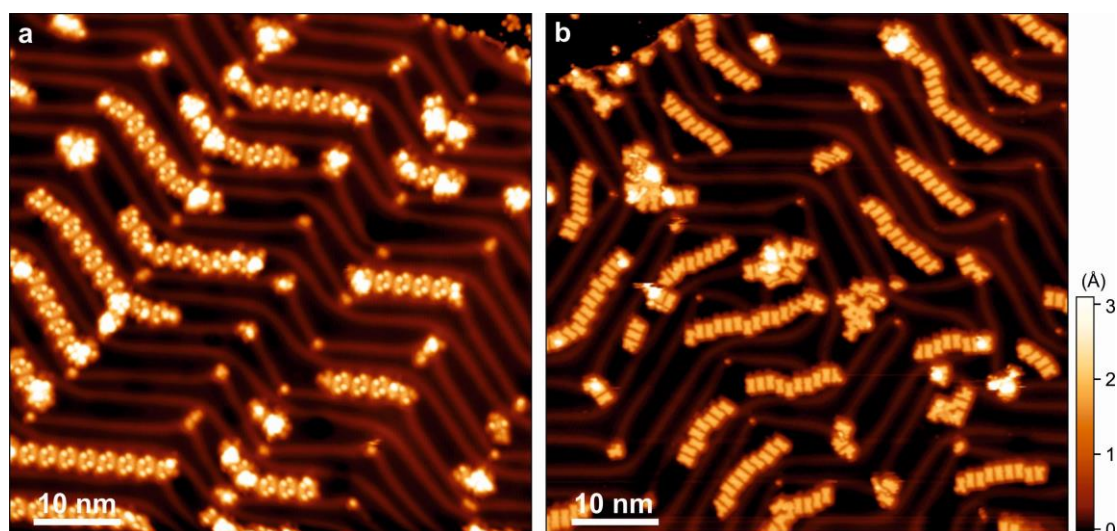
4. Scanning Tunneling Microscopy

Figure S2. (a) STM image of precursor **2** deposited on Au(111) held at room temperature (tunneling parameters: −2.0 V, 100 pA). (b) STM image of product **1** after annealing to 380 °C (tunneling parameters: 0.6 V, 20 pA).
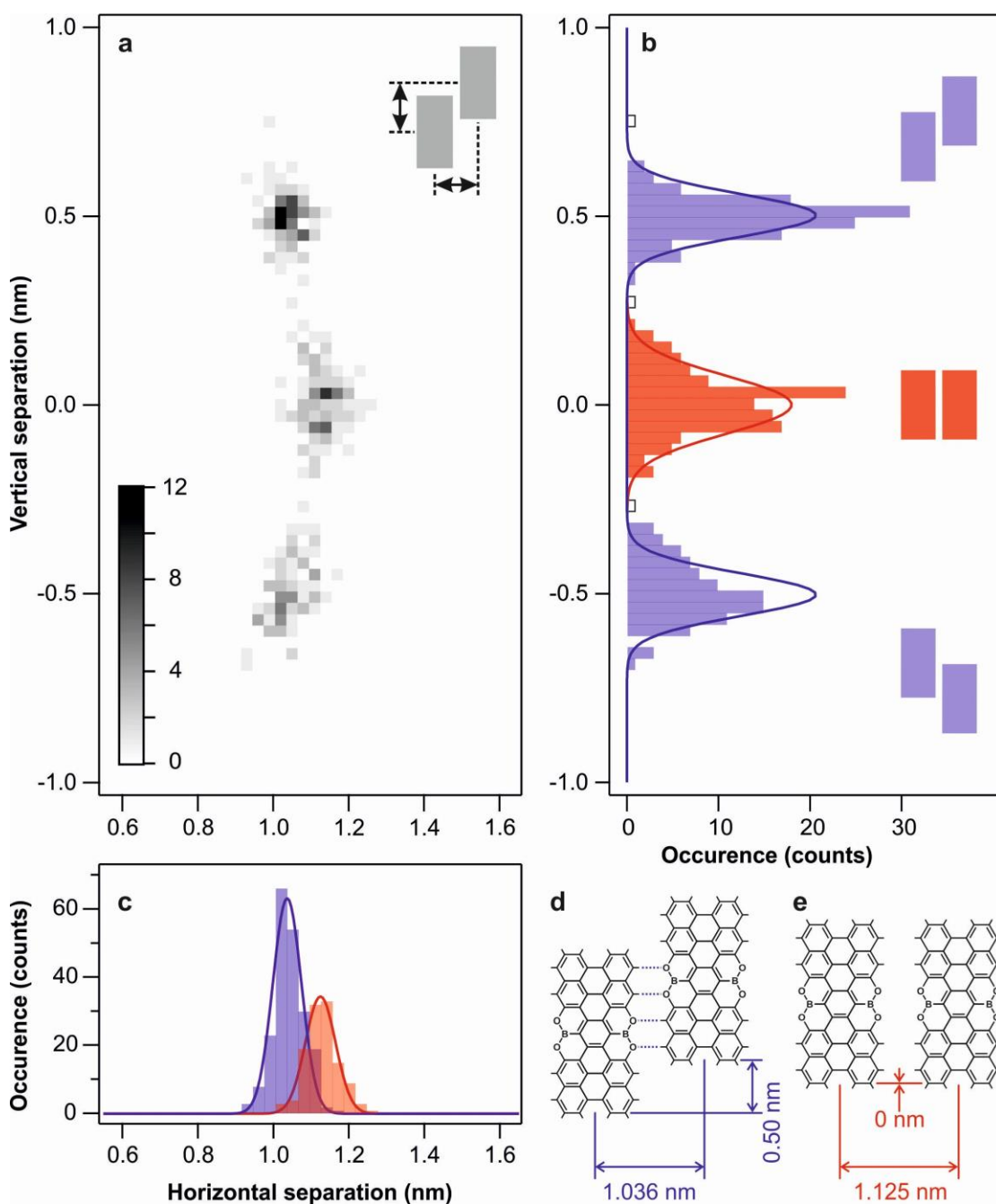
Figure S3. Separation analysis for neighboring perihexacene analogue **1** on Au(111). (a) Distribution map for 326 molecule pairs. (b) Histogram of the vertical separation, with highlighted areas for "abreast" (red) and "stepped" arrangement (blue). (c) Horizontal distribution of molecules in the two regions highlighted in (b) with the corresponding Gauss fits (stepped assembly in blue, abreast assembly in red). Molecular models of (d) the stepped arrangement and (e) the abreast arrangement with vertical and horizontal separation distances. The peripheral short bonds indicate C−H bonds where the hydrogen atoms are omitted for clarity.

Both species, precursor **2** and perihexacene analogue **1**, assemble into chains on the Au(111) surface (Figure S2). In the case of the latter the arrangement along each chain occurs in two different fashions, namely the "stepped" and the "abreast" arrangement. To investigate the differences for the two packing schemes in more detail, we measured the distances within all chains in an STM image of 120×120 nm^2 (containing 73 chains, *i.e.*, dimers to oligomers, incorporating 326 separations). Figure S3a shows the distribution map of the horizontal separation (along the chain) and the vertical separation (perpendicular to the chain) between neighboring molecules. Three distinct areas can be observed. Integrating the number of molecules with the same vertical separation reveals three clear maxima assignable to the abreast and the stepped arrangements, highlighted in red and blue, respectively (Figure S3b). A Gauss fit to the latter reveals an average separation of 0.5 nm, corresponding to an upshift of approximately two zigzag cusps, which can be associated with the formation of four O···H hydrogen bonds (up and down shifts are equivalent in case of the symmetric molecule). Next, the distances of the two species are analyzed for their horizontal separation. Figure S3c shows the two histograms and the corresponding fits to the data points, revealing a separation of 1.036 nm for the stepped and 1.125 nm for the abreast arranged molecules. With this information the bond length of the O···H hydrogen bonds present in the stepped case can be determined to be 0.19 nm and the O···O distance in the abreast case 0.40 nm. The latter translates into an O···Au distance of 0.235 nm for the coordinating Au adatom, which is well within the range expected for metal coordination.

5. Scanning Tunneling Spectroscopy
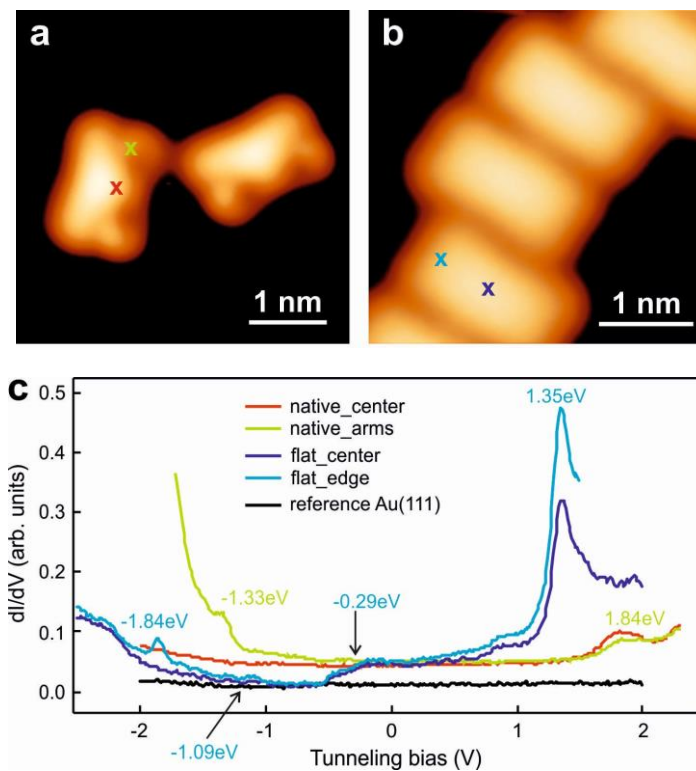
Figure S4. Differential conductance (d*I*/d*V*) spectra (c) of precursor **2** and perihexacene analogue **1** with the corresponding positions indicated in the STM images (a,b). Tunneling parameters: (a) 300 mV, 100 pA; (b) 100 mV, 30 pA.

6. Fast XPS Mapping
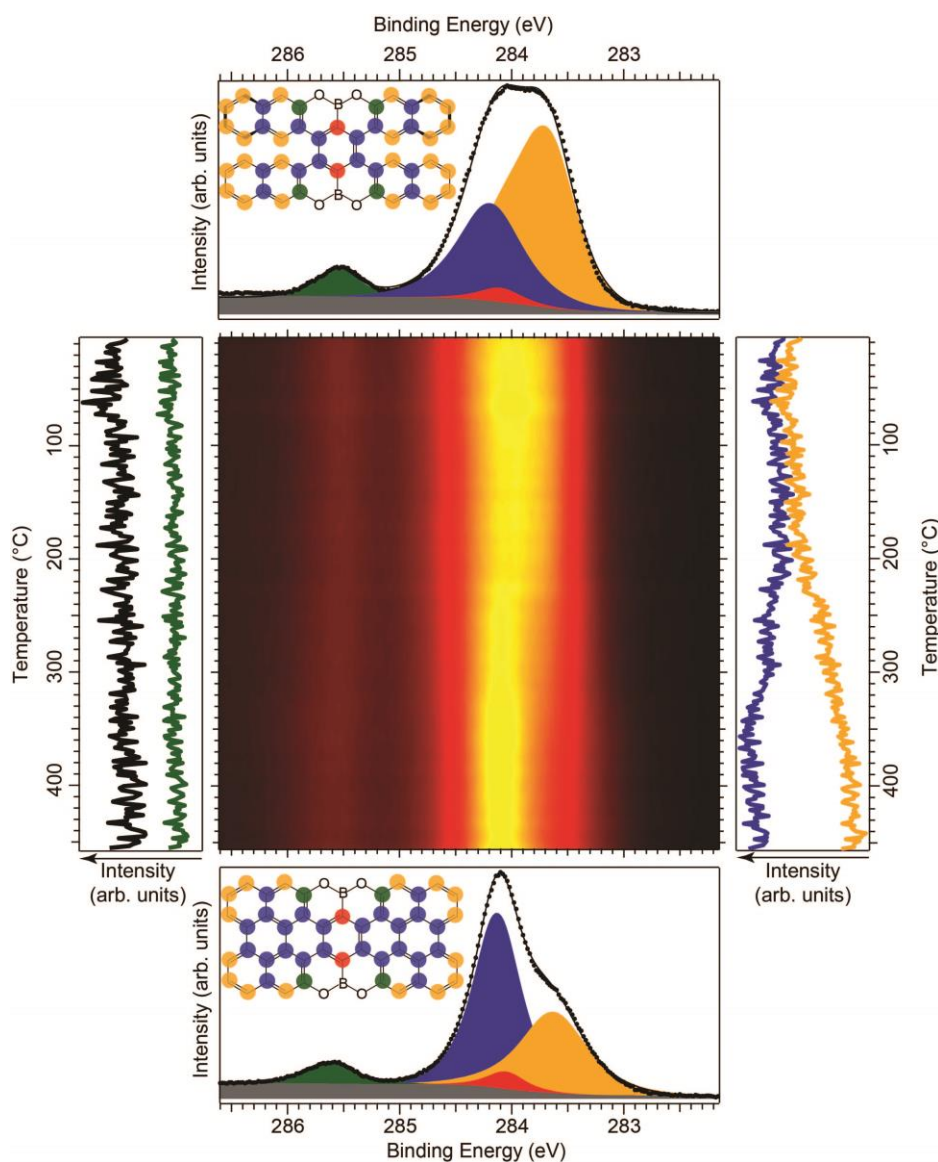
Figure S5. Fast XPS mapping for the C 1s level of **2** deposited on Au(111) and annealed with a heating rate of 0.2 °C s^{-1} (central panel, pass energy = 50 eV). High-resolution C 1s spectra (pass energy = 20 eV) acquired before and after the heating ramp (top and bottom panels) together with representative schemes of the molecule in the two phases. Vertical profiles representing the change of the C–C and C–H components (blue and orange, respectively) are reported in the right panel. The C–O component (green) and the total area of each spectrum (black) are not significantly changing during the annealing, as shown by the curves reported in the left panel.

7. Theoretical Simulations

7.1 Gas-phase quantum chemistry calculations. The geometries were optimized in the gas phase at the B3LYP/6-311G(d,p) level of theory using the Gaussian 09 software package.[6] Frequencies were calculated for each geometry to confirm the local energy minimum or the transition state. The rate constant (k) at room temperature (298.15 K) was estimated using the Eyring equation[7]

$$k = \kappa(k_B T/h)\exp(-\Delta G^{\ddagger}/RT)$$

where k is the rate constant; κ is the transmission coefficient which is taken to be unity; k_B is the Boltzmann constant; T is the temperature; h is the Planck constant; $\Delta G^{\ddagger}$ is the Gibbs energy of activation; R is the gas constant.
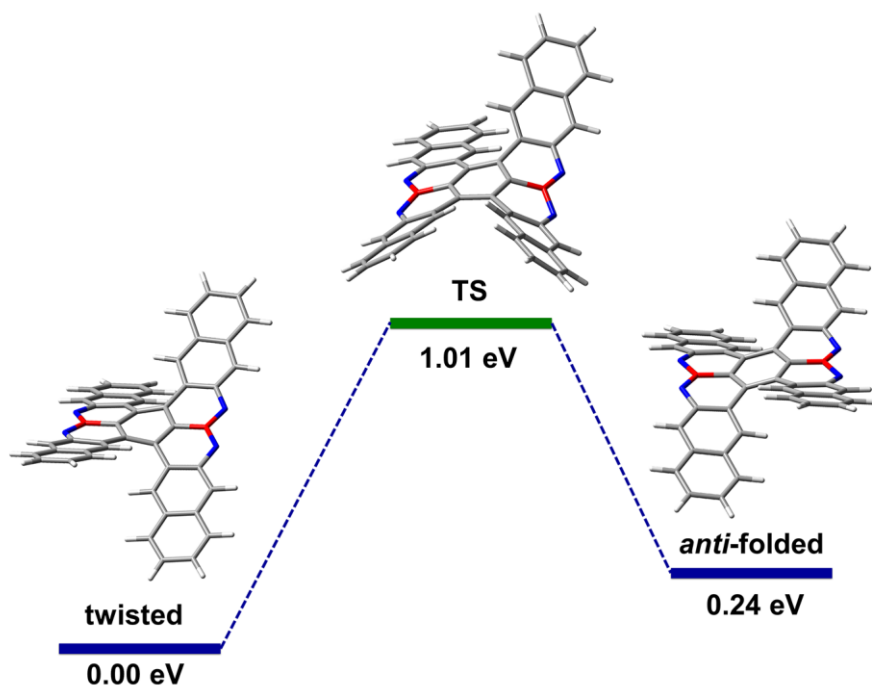
Figure S6. Isomerization process of compound **2** from the twisted to the *anti*-folded conformation. The relative Gibbs free energies were calculated at the B3LYP/6-311G(d,p) level. As estimated from the Eyring equation, the rate constants for the forward isomerization (k_f, from twisted **2** to *anti*-foled **2**) and the backward reaction (k_b, from *anti*-folded **2** to twisted **2**) are 4.7×10^{-5} s^{-1} and 5.8×10^{-1} s^{-1}, respectively. Therefore, the thermodynamic equilibrium constant K ($= k_f/k_b$) of the forward reaction is 8.1×10^{-5}, indicating that compound **2** dominantly adopts the twisted conformation at the equilibrium state at room temperature.
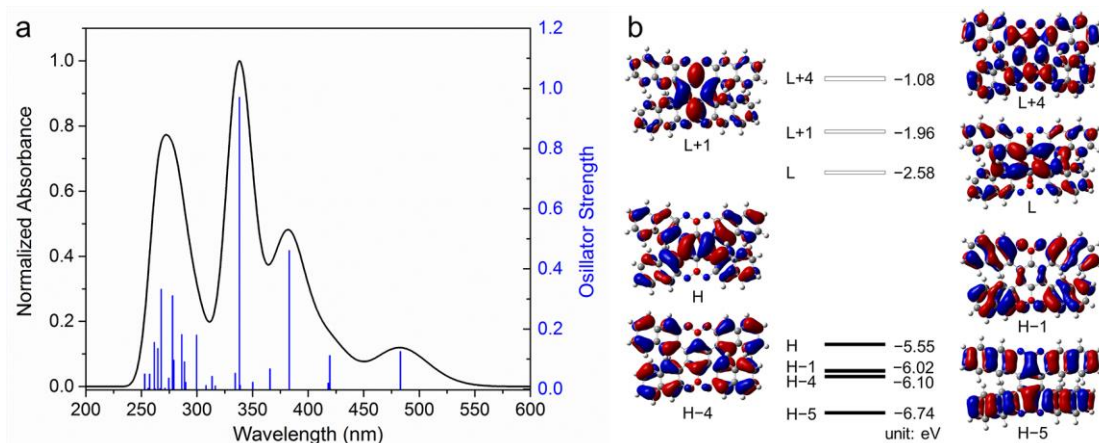
Figure S7. (a) The simulated absorption spectrum of compound **2** (Gaussian line shape, half-width: 0.15 eV) and the oscillator strengths (blue bars) by TDDFT calculations at the B3LYP/6-311G(d,p) level. The twisted conformation was used since it dominantly exists at the equilibrium state. (b) Selected molecular orbitals and energy levels of **2** calculated at the B3LYP/6-311G(d,p) level. H: HOMO; L: LUMO.

Table S1. Selected electronic transitions of **2** calculated by TDDFT method.

Excited State	Energy (eV)	Wavelength (nm)	Oscillator Strength	Configuration
1	2.57	483	0.1258	HOMO→LUMO (0.70534)
2	2.96	420	0.1121	HOMO–1→LUMO (0.69904)
3	3.24	383	0.4612	HOMO–5→LUMO (–0.14374) HOMO–4→LUMO (0.47269) HOMO→LUMO+1 (0.48195)
4	3.67	338	0.9707	HOMO–5→LUMO (0.59951) HOMO–1→LUMO+1 (0.24188) HOMO→LUMO+1 (0.14698) HOMO→LUMO+4 (–0.11746)
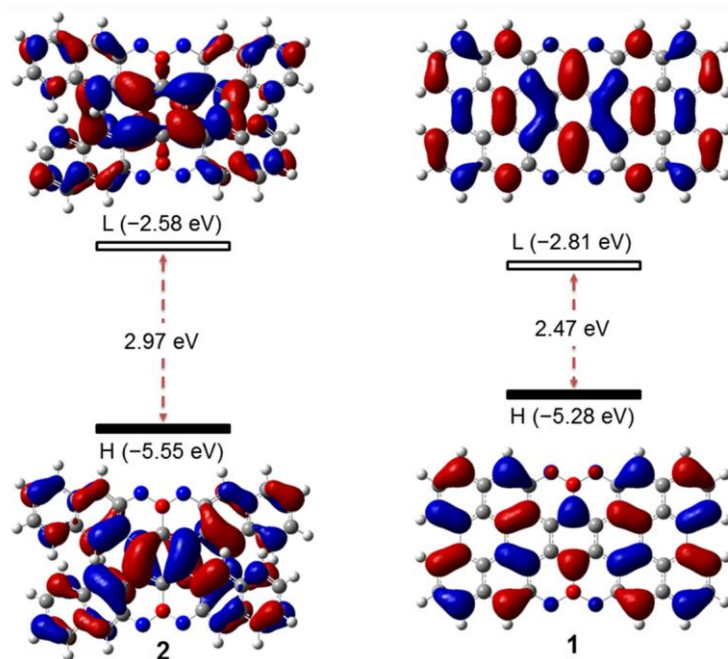
Figure S8. Frontier molecular orbitals of compounds **2** and **1** and associated energy levels according to DFT calculations at the B3LYP/6-311G(d,p) level, showing that **1** has a lower HOMO-LUMO gap than **2**. H: HOMO; L: LUMO.

7.2 On-Surface Simulations. DFT calculations were performed using the Vienna Ab initio simulation package (VASP)[8] using the projector augmented wave (PAW) method[9] and the optB86b-vdW functional, which includes long-range van der Waals (vdW) interactions.[10] Considering the large size of the supercells, the *k*-point sampling was restricted to the Γ point. A plane-wave cutoff of 400 eV was used. The vacuum regions in all the calculations were larger than 10 Å. We used a four layer thick rectangular 8×5 Au(111) slab in the calculations involving isolated molecules while a four layer thick rectangular 8×4 Au(111) slab was used in the calculations involving hydrogen bonded chains of precursor **2**. The smallest distance between any two atoms in a molecule and its periodic image was larger than 4.5 Å, ensuring minimal interaction.

The energy barriers for the isomerization process of precursor **2** from the twisted to the *anti*-folded conformation were calculated using the climbing-image nudged elastic band (NEB) method.[11] We used 16 intermediate structures in our NEB calculations. The bottom two layers in the Au slab were fixed throughout the NEB

calculations while remainder of the atomic coordinates were relaxed using a conjugate-gradient algorithm until all forces were smaller in magnitude than 0.05 eV/Å.

Table S2. Energetics of precursor 2 as single molecules.[a]

	Total energy (eV)		Binding energy (eV)
	Gas phase	Substrate-supported	
T	-482.73	-659.79	3.75
A	-482.55	-659.82	3.96

[a] T: twisted conformation of **2**; A: *anti*-folded conformation of **2**.

Table S3. Energetics of hydrogen bonded chains of precursor 2.[a]

	Total energy (eV)		Binding energy (eV)
	Gas phase	Substrate-supported	
TT	-966.12	-1065.59	7.31
AA	-965.52	-1065.88	8.20

[a] The chains are labeled as TT or AA depending on the conformations of the monomers in the smallest repeating units. The energies shown in this table are for the repeating units, that is, the dimers TT and AA.

Table S4. Binding energies of hydrogen-bonds in chains of precursor 2.[a]

	Gas phase	Substrate-supported
TT	0.71	0.70
AA	0.61	0.75

[a] The chains are labeled as TT or AA depending on the conformations of the monomers in the smallest repeating units.
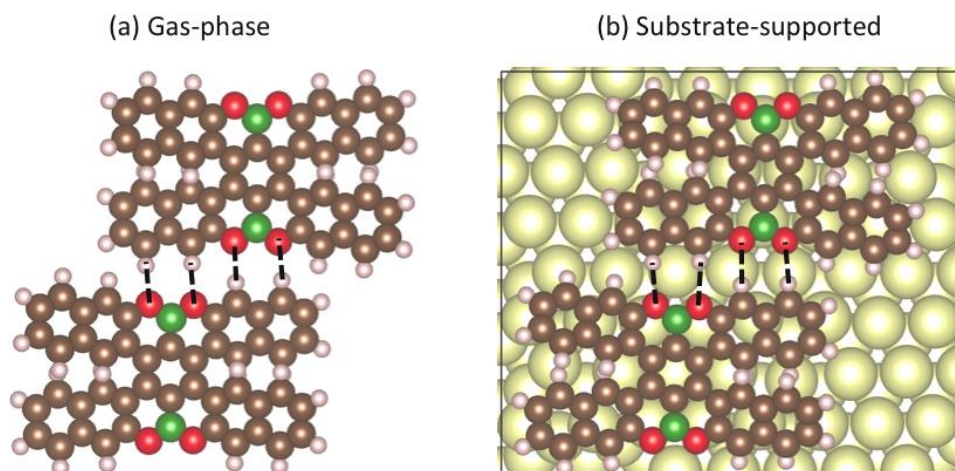
Figure S9. Atomistic schematics of the hydrogen-bonded chains of precursor **2** in the (a) gas-phase and (b) substrate-supported configurations. Hydrogen bonds are depicted by black dashed lines.
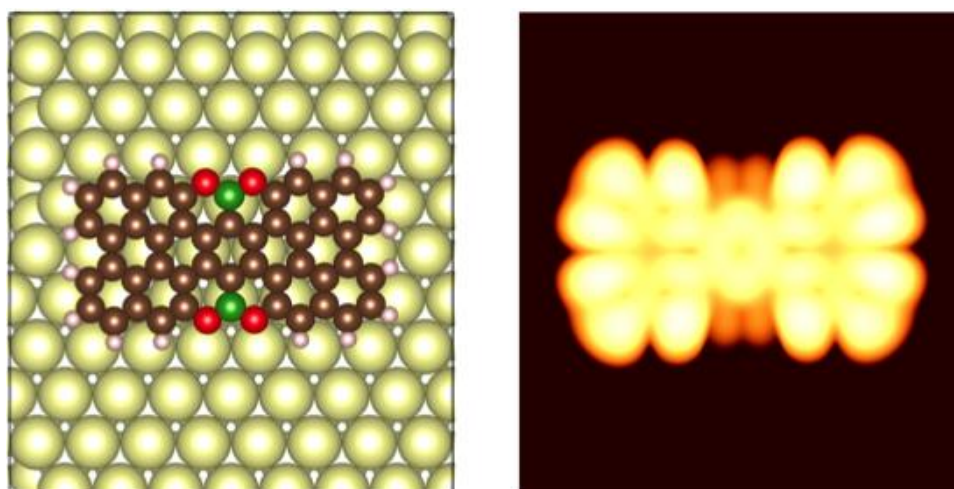
Figure S10. Atomistic schematic of perihexacene analogue **1** (left) and its DFT-simulated STM image (right).

7.3 Assignment of the Main Raman Transitions. The DFT calculations of the Raman spectra of **1** and **2** reported in the main text have been carried out at the B3LYP/6-31G(d,p) level in pre-resonance conditions by using the Gaussian 09 program[6] and by adopting the excitation wavelengths of 520 nm (**1**) and 530 nm (**2**). These wavelengths were selected because they best reproduced the experimental

observation after systematic inspection of the results of the simulations carried out over a wide range of excitation wavelengths (400–560 nm). The selected wavelengths are both close to the excitation wavelength adopted in the experiments (532 nm). The slight difference between the excitation wavelength selected for **1** *vs*. **2** (*i.e.*, 520 *vs.* 530 nm) can be ascribed to the different experimental conditions adopted for recording the spectra of the two molecules (**1** adsorbed on gold *vs.* **2** as powder). As customary, wavenumbers in all simulated spectra have been uniformly scaled by 0.98 to ease the comparison with experiments. The twisted conformation of **2** was used for these simulations since this is the expected structure of the molecule in the measured powder samples.
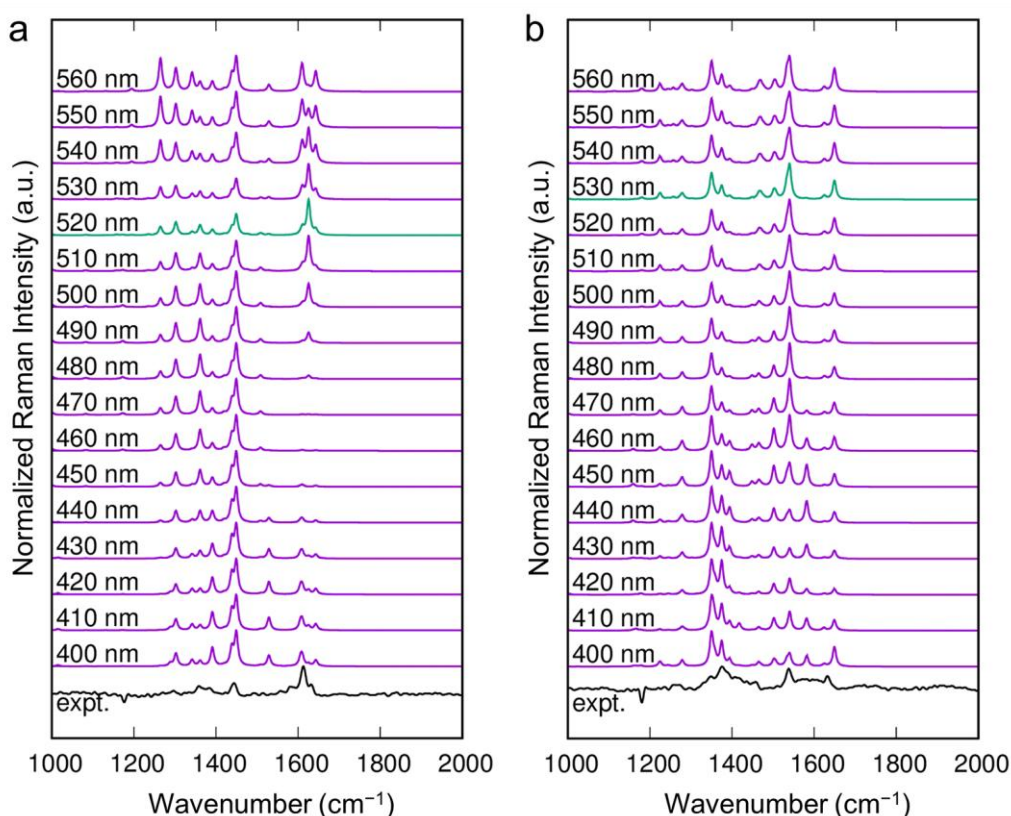
Figure S11. Simulated Raman spectra of (a) **1** and (b) **2** as a function of the excitation wavelength. The spectra selected for Figure 3 in the main text are drawn with green lines. The observed line shape of the G band of **1** is the result of an excitation located around 520-530 nm: a weak G signal is obtained for excitations below 500 nm, and above 530 nm the line shape of the G band significantly deviates from the experimental observation. In contrast, the relative intensities of the simulated spectra of **2** are less affected by the choice of the excitation wavelength around 530 nm.
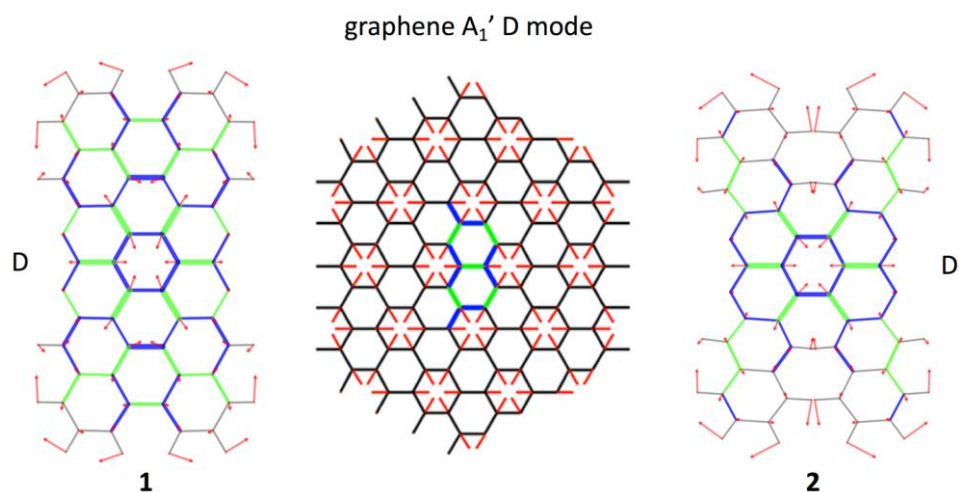
graphene A$_1$' D mode

Figure S12. Assignment of the D modes of **1** and **2** based on the nuclear displacements computed for graphene (adapted from the literature[12]). Red arrows (or sticks) represent displacement vectors; CC bonds are represented as green (blue) lines of different thickness according to their relative stretching (shrinking).

graphene E$_{2g}$ G-mode
(doubly degenerate)

longitudinal displacements

transversal displacements
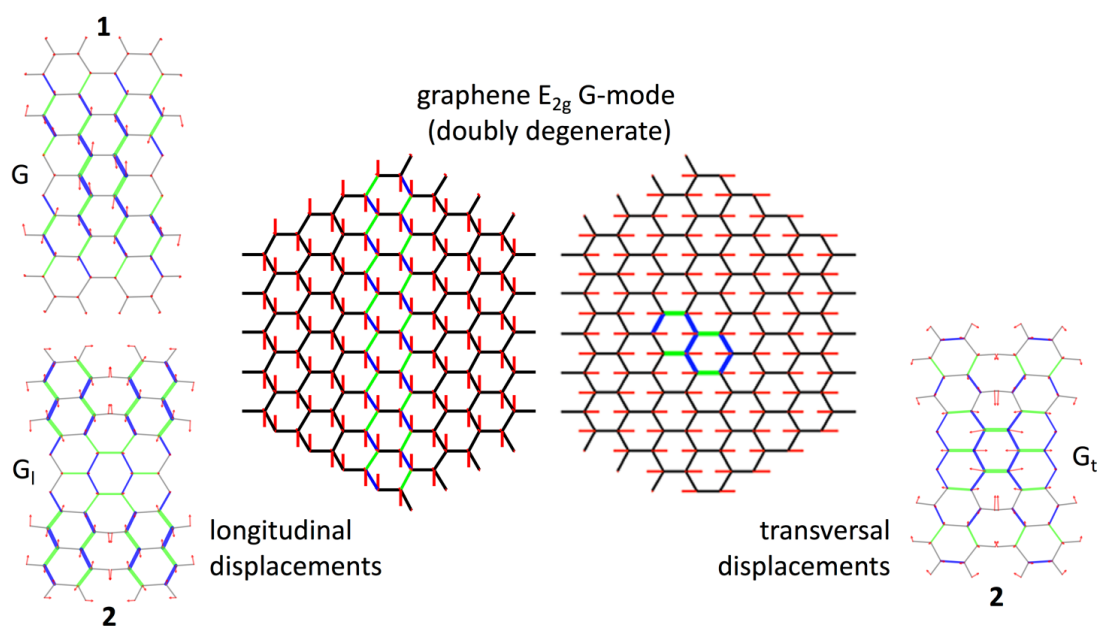
Figure S13. Assignment of the G modes of **1** and **2** based on the nuclear displacements computed for graphene (adapted from the literature[12]). Red arrows (or sticks) represent displacement vectors; CC bonds are represented as green (blue) lines of different thickness according to their relative stretching (shrinking).

Figure S12 and S13 show the nuclear displacements of the normal modes of **1** and **2** assigned to the relevant observed Raman lines. The D modes of **1** and **2** are

computed respectively at 1479 and 1378 cm^{-1}; the associated nuclear displacement patterns at the center of the molecule closely match the characteristic D mode of graphene (Figure S12). Interestingly, the Raman spectrum of **2** shows one transversal G mode (G$_t$, computed at 1572 cm^{-1}) and one longitudinal G mode (G$_l$, computed at 1683 cm^{-1}). This naming scheme has been adopted after inspecting the direction of the displacements of the π-conjugated carbon atoms with respect to the shape of the molecule (Figure S13). In molecule **1** the observed G peak is longitudinal (computed at 1659 cm^{-1}) and the associated transversal component (computed at 1677 cm^{-1}) is comparatively weak. The latter is predicted and observed as the higher wavenumber shoulder of the G line (see Figure 3 in the main text). Based on DFT calculations, the lower wavenumber shoulder of the G line of **1** is computed at 1643 cm^{-1} and the associated normal mode displays a collective ring stretching pattern not directly related with graphene G mode.

Appendix:
**Cartesian coordinates obtained in gas-phase DFT calculations at the B3LYP/6-311G(d,p) level**

Optimized twisted **2**

Tag	Symbol	X	Y	Z
1	C	-1.240631	0.696511	0.146523
2	C	-1.240631	-0.696511	-0.146525
3	C	0.000007	-1.353736	-0.000012
4	C	1.240644	-0.696513	0.146513
5	C	1.240645	0.696514	-0.146514
6	C	0.000007	1.353736	0.000011
7	C	-2.372390	1.507763	0.638123
8	C	2.372399	1.507775	-0.638111
9	C	-2.275227	2.939906	0.661540
10	C	-3.299037	3.728744	1.127589
11	C	-4.475701	3.157127	1.656370
12	C	-4.567064	1.730525	1.723302
13	C	-3.505948	0.952830	1.216840
14	C	3.505953	0.952855	-1.216850
15	C	4.567063	1.730559	-1.723307
16	C	4.475700	3.157160	-1.656349
17	C	3.299039	3.728766	-1.127549
18	C	2.275234	2.939918	-0.661506
19	C	-2.372390	-1.507764	-0.638124
20	C	2.372399	-1.507775	0.638110
21	C	2.275235	-2.939918	0.661501
22	C	3.299040	-3.728766	1.127544
23	C	4.475699	-3.157160	1.656348
24	C	4.567061	-1.730559	1.723311
25	C	3.505950	-0.952855	1.216853
26	C	-3.505951	-0.952830	-1.216837
27	C	-4.567067	-1.730525	-1.723298
28	C	-4.475702	-3.157127	-1.656371
29	C	-3.299036	-3.728744	-1.127595
30	C	-2.275225	-2.939906	-0.661547
31	B	0.000005	2.880034	0.000021
32	B	0.000007	-2.880034	-0.000027
33	O	-1.140006	3.590827	0.249379
34	O	1.140012	3.590832	-0.249334
35	O	-1.140003	-3.590827	-0.249390
36	O	1.140015	-3.590832	0.249324

Tag	Symbol	X	Y	Z
37	C	-5.553233	3.937817	2.152209
38	C	-6.663181	3.335707	2.690902
39	C	-6.752729	1.923357	2.764028
40	C	-5.729201	1.140860	2.293168
41	C	-5.729207	-1.140860	-2.293159
42	C	-6.752734	-1.923357	-2.764019
43	C	-6.663184	-3.335707	-2.690898
44	C	-5.553234	-3.937817	-2.152209
45	C	5.553226	-3.937860	2.152183
46	C	6.663168	-3.335761	2.690901
47	C	6.752714	-1.923412	2.764057
48	C	5.729191	-1.140906	2.293202
49	C	5.729196	1.140905	-2.293194
50	C	6.752719	1.923412	-2.764049
51	C	6.663171	3.335760	-2.690897
52	C	5.553227	3.937859	-2.152183
53	H	-3.168290	4.804239	1.108007
54	H	-3.591124	-0.123331	1.286069
55	H	3.591128	-0.123305	-1.286102
56	H	3.168289	4.804260	-1.107950
57	H	3.168292	-4.804261	1.107942
58	H	3.591124	0.123305	1.286108
59	H	-3.591128	0.123331	-1.286062
60	H	-3.168286	-4.804239	-1.108017
61	H	-5.483753	5.019157	2.101086
62	H	-7.479659	3.942113	3.066664
63	H	-7.635847	1.464603	3.193682
64	H	-5.794643	0.059166	2.343221
65	H	-5.794650	-0.059165	-2.343208
66	H	-7.635854	-1.464602	-3.193669
67	H	-7.479663	-3.942112	-3.066659
68	H	-5.483753	-5.019157	-2.101091
69	H	5.483747	-5.019199	2.101038
70	H	7.479642	-3.942173	3.066659
71	H	7.635827	-1.464667	3.193731
72	H	5.794632	-0.059212	2.343278
73	H	5.794639	0.059212	-2.343266
74	H	7.635833	1.464666	-3.193719
75	H	7.479645	3.942173	-3.066655
76	H	5.483746	5.019199	-2.101042

Optimized *anti*-folded 2

Tag	Symbol	X	Y	Z
1	C	-1.251802	0.701919	-0.103978
2	C	-1.251802	-0.701921	0.103975
3	C	0.000001	-1.334466	0.272765
4	C	1.251803	-0.701921	0.103975
5	C	1.251803	0.701920	-0.103977
6	C	0.000000	1.334465	-0.272767
7	C	-2.422582	1.614656	-0.073800
8	C	2.422582	1.614657	-0.073795
9	C	-2.338269	2.899367	-0.705748
10	C	-3.399065	3.771292	-0.725974
11	C	-4.600765	3.467346	-0.050888
12	C	-4.675029	2.241460	0.682978
13	C	-3.576392	1.356166	0.650551
14	C	3.576392	1.356166	0.650556
15	C	4.675028	2.241460	0.682986
16	C	4.600765	3.467347	-0.050877
17	C	3.399066	3.771295	-0.725964
18	C	2.338270	2.899369	-0.705740
19	C	-2.422582	-1.614658	0.073797
20	C	2.422582	-1.614658	0.073794
21	C	2.338271	-2.899370	0.705740
22	C	3.399067	-3.771294	0.725964
23	C	4.600767	-3.467346	0.050878
24	C	4.675030	-2.241459	-0.682985
25	C	3.576392	-1.356166	-0.650557
26	C	-3.576393	-1.356167	-0.650551
27	C	-4.675031	-2.241459	-0.682976
28	C	-4.600767	-3.467346	0.050888
29	C	-3.399066	-3.771294	0.725971
30	C	-2.338269	-2.899369	0.705744
31	B	0.000001	2.722907	-0.920495
32	B	0.000001	-2.722909	0.920491
33	O	-1.167845	3.339304	-1.273767
34	O	1.167846	3.339308	-1.273758
35	O	-1.167844	-3.339309	1.273759
36	O	1.167847	-3.339309	1.273757
37	C	-5.715786	4.346158	-0.033871
38	C	-6.845681	4.028591	0.678634
39	C	-6.918678	2.818265	1.411380
40	C	-5.858487	1.947297	1.414212
41	C	-5.858490	-1.947295	-1.414208
42	C	-6.918682	-2.818261	-1.411375
43	C	-6.845684	-4.028588	-0.678630
44	C	-5.715789	-4.346157	0.033872
45	C	5.715788	-4.346158	0.033860

Tag	Symbol	X	Y	Z
46	C	6.845683	-4.028589	-0.678645
47	C	6.918679	-2.818262	-1.411389
48	C	5.858487	-1.947295	-1.414219
49	C	5.858486	1.947296	1.414221
50	C	6.918677	2.818263	1.411391
51	C	6.845680	4.028591	0.678648
52	C	5.715786	4.346159	-0.033857
53	H	-3.274819	4.720997	-1.232674
54	H	-3.654087	0.437241	1.215132
55	H	3.654087	0.437240	1.215136
56	H	3.274820	4.721001	-1.232661
57	H	3.274822	-4.721000	1.232662
58	H	3.654088	-0.437240	-1.215137
59	H	-3.654090	-0.437241	-1.215131
60	H	-3.274819	-4.720999	1.232670
61	H	-5.658871	5.275653	-0.590228
62	H	-7.690746	4.707876	0.684758
63	H	-7.817924	2.583494	1.969226
64	H	-5.911455	1.017103	1.969786
65	H	-5.911459	-1.017100	-1.969781
66	H	-7.817929	-2.583490	-1.969219
67	H	-7.690750	-4.707873	-0.684753
68	H	-5.658873	-5.275652	0.590228
69	H	5.658874	-5.275653	0.590215
70	H	7.690748	-4.707874	-0.684770
71	H	7.817924	-2.583490	-1.969236
72	H	5.911455	-1.017099	-1.969792
73	H	5.911454	1.017100	1.969793
74	H	7.817922	2.583492	1.969238
75	H	7.690745	4.707876	0.684774
76	H	5.658871	5.275655	-0.590213

Optimized TS-2

Tag	Symbol	X	Y	Z
1	C	1.241943	-0.588274	0.091458
2	C	0.011388	-1.229358	-0.139474
3	C	-1.261624	-0.618745	-0.048011
4	C	-1.275076	0.804763	0.182985
5	C	-0.009965	1.465077	0.080498
6	C	1.250726	0.823853	0.007101
7	C	-2.443988	1.719345	0.374757
8	C	-2.332148	3.126067	0.070234
9	C	-3.679227	1.355561	0.890616
10	C	-3.403493	3.984995	0.096241
11	C	-4.798896	2.212935	0.972502
12	C	-4.677283	3.558674	0.518875
13	C	-2.371537	-1.586550	-0.349702
14	C	-3.592141	-1.705980	0.295048
15	C	-2.132547	-2.611574	-1.342049
16	C	-4.634626	-2.561748	-0.135327
17	C	-3.132029	-3.408197	-1.838947
18	C	-4.430450	-3.378660	-1.286092
19	C	2.452525	1.647647	-0.291210
20	C	2.367231	3.077395	-0.269691
21	C	3.670849	1.123059	-0.706930
22	C	3.454748	3.886946	-0.495794
23	C	4.803872	1.919340	-0.973391
24	C	4.708466	3.339125	-0.832624
25	C	2.379663	-1.496193	0.357980
26	C	3.378316	-1.206155	1.271120
27	C	2.390915	-2.792515	-0.243420
28	C	4.425297	-2.110485	1.555052
29	C	3.403148	-3.689068	-0.012332
30	C	4.451641	-3.374733	0.882712
31	B	0.011182	2.988235	-0.055784
32	B	0.169190	-2.521193	-0.953596
33	O	1.169745	3.708514	-0.090243
34	O	-1.130118	3.712716	-0.202120
35	O	1.364874	-3.173552	-1.073175
36	O	-0.860483	-2.929434	-1.753297
37	H	-3.224543	5.020151	-0.168952
38	H	-3.811230	0.376143	1.294072
39	H	3.311266	4.960075	-0.452698
40	H	3.780461	0.058062	-0.835561
41	H	3.369484	-0.249300	1.779715
42	H	3.369781	-4.652362	-0.507461
43	H	-2.873250	-4.129691	-2.604782
44	H	-3.764330	-1.185462	1.218818
45	C	5.514181	-4.274869	1.158539
46	C	6.499801	-3.942527	2.055108
47	C	6.473290	-2.694073	2.723053
48	C	5.459759	-1.801454	2.479758
49	H	5.436978	-0.842883	2.987215
50	H	5.533680	-5.232786	0.649875
51	H	7.305717	-4.639098	2.256979
52	H	7.258842	-2.446934	3.427857
53	C	6.045586	1.348659	-1.368725
54	C	7.138828	2.143607	-1.601750

Tag	Symbol	X	Y	Z
55	H	8.082002	1.699580	-1.898701
56	C	7.043300	3.550092	-1.454279
57	H	7.915656	4.166239	-1.641451
58	C	5.858713	4.134302	-1.080796
59	H	5.784870	5.211270	-0.974195
60	H	6.114747	0.271309	-1.475175
61	C	-5.884976	-2.618988	0.534616
62	C	-6.896662	-3.420601	0.064950
63	H	-7.850617	-3.451306	0.578648
64	C	-6.700275	-4.208381	-1.094058
65	H	-7.508025	-4.833346	-1.458000
66	C	-5.494066	-4.192794	-1.752151
67	H	-5.337671	-4.809539	-2.630628
68	H	-6.034547	-2.011874	1.421457
69	C	-5.809700	4.412303	0.571182
70	C	-7.006398	3.950652	1.061664
71	H	-7.867467	4.608563	1.097580
72	C	-7.127483	2.618632	1.527669
73	H	-8.078560	2.271241	1.914547
74	C	-6.048277	1.771670	1.486285
75	H	-6.141398	0.749163	1.836278
76	H	-5.713761	5.434977	0.222642

Optimized 1

Tag	Symbol	X	Y	Z
1	C	-1.213412	0.705859	0.000263
2	C	-1.213412	-0.705859	0.000264
3	C	0.000000	-1.389250	0.000330
4	C	1.213412	-0.705859	0.000262
5	C	1.213412	0.705859	0.000262
6	C	0.000000	1.389250	0.000329
7	C	-2.431969	1.433865	0.000107
8	C	2.431969	1.433865	0.000106
9	C	-2.406833	2.866436	-0.000053
10	C	-3.586809	3.558198	-0.000081
11	C	-4.837807	2.869294	-0.000028
12	C	-4.876402	1.436876	-0.000007
13	C	-3.646899	0.724744	0.000074
14	C	3.646899	0.724744	0.000073
15	C	4.876402	1.436876	-0.000008
16	C	4.837807	2.869294	-0.000028
17	C	3.586809	3.558198	-0.000081
18	C	2.406833	2.866436	-0.000054
19	C	-2.431969	-1.433865	0.000108
20	C	2.431969	-1.433865	0.000106
21	C	2.406833	-2.866436	-0.000054
22	C	3.586809	-3.558198	-0.000081
23	C	4.837807	-2.869294	-0.000028
24	C	4.876402	-1.436876	-0.000008
25	C	3.646899	-0.724744	0.000073
26	C	-3.646899	-0.724744	0.000074
27	C	-4.876402	-1.436876	-0.000007
28	C	-4.837807	-2.869294	-0.000028
29	C	-3.586809	-3.558198	-0.000081
30	C	-2.406833	-2.866436	-0.000053
31	B	0.000000	2.898955	0.000125
32	B	0.000000	-2.898955	0.000125
33	O	-1.209225	3.566602	-0.000091
34	O	1.209225	3.566602	-0.000092
35	O	-1.209225	-3.566602	-0.000091
36	O	1.209225	-3.566602	-0.000092
37	C	-6.059188	3.576001	-0.000072
38	C	-7.258603	2.894146	-0.000096
39	C	-7.293138	1.493675	-0.000077
40	C	-6.122997	0.737773	-0.000046
41	C	-6.122997	-0.737773	-0.000046
42	C	-7.293137	-1.493675	-0.000078
43	C	-7.258603	-2.894146	-0.000097
44	C	-6.059188	-3.576001	-0.000072
45	C	6.122997	0.737773	-0.000046
46	C	7.293137	1.493675	-0.000077
47	C	7.258603	2.894146	-0.000096
48	C	6.059188	3.576001	-0.000071
49	C	6.059188	-3.576001	-0.000071
50	C	7.258603	-2.894146	-0.000096
51	C	7.293137	-1.493675	-0.000077
52	C	6.122997	-0.737773	-0.000046
53	H	-3.569915	4.641503	-0.000143
54	H	3.569915	4.641503	-0.000143
55	H	3.569915	-4.641503	-0.000143
56	H	-3.569915	-4.641503	-0.000143
57	H	-6.042574	4.660227	-0.000097
58	H	-8.192099	3.445611	-0.000130
59	H	-8.258680	1.005355	-0.000096
60	H	-8.258680	-1.005355	-0.000096
61	H	-8.192099	-3.445611	-0.000130
62	H	-6.042574	-4.660227	-0.000097
63	H	8.258680	1.005355	-0.000096

64	H	8.192099	3.445611	-0.000129	67	H	8.192099	-3.445611	-0.000129
65	H	6.042574	4.660227	-0.000096	68	H	8.258680	-1.005355	-0.000096
66	H	6.042574	-4.660227	-0.000096					

8. References

(1) Suzuki, K.; Kobayashi, A.; Kaneko, S.; Takehira, K.; Yoshihara, T.; Ishida, H.; Shiina, Y.; Oishi, S.; Tobita, S. *Phys. Chem. Chem. Phys.* **2009**, *11*, 9850.

(2) Giessibl, F. J. *Appl. Phys. Lett.* **2000**, *76*, 1470.

(3) Bartels, L.; Meyer, G.; Rieder, K. H.; Velic, D.; Knoesel, E.; Hotzel, A.; Wolf, M.; Ertl, G. *Phys. Rev. Lett.* **1998**, *80*, 2004.

(4) Muntwiler, M.; Zhang, J.; Stania, R.; Matsui, F.; Oberta, P.; Flechsig, U.; Patthey, L.; Quitmann, C.; Glatzel, T.; Widmer, R.; Meyer, E.; Jung, T. A.; Aebi, P.; Fasel, R.; Greber, T. *J. Synchrotron Rad.* **2017**, *24*, 354.

(5) Niimi, K.; Mori, H.; Miyazaki, E.; Osaka, I.; Kakizoe, H.; Takimiya, K.; Adachi, C. *Chem. Commun.* **2012**, *48*, 5892.

(6) Gaussian 09, Revision D.01, Frisch, M. J.; Trucks, G. W.; Schlegel, H. B.; Scuseria, G. E.; Robb, M. A.; Cheeseman, J. R.; Scalmani, G.; Barone, V.; Mennucci, B.; Petersson, G. A.; Nakatsuji, H.; Caricato, M.; Li, X.; Hratchian, H. P.; Izmaylov, A. F.; Bloino, J.; Zheng, G.; Sonnenberg, J. L.; Hada, M.; Ehara, M.; Toyota, K.; Fukuda, R.; Hasegawa, J.; Ishida, M.; Nakajima, T.; Honda, Y.; Kitao, O.; Nakai, H.; Vreven, T.; Montgomery, Jr., J. A.; Peralta, J. E.; Ogliaro, F.; Bearpark, M.; Heyd, J. J.; Brothers, E.; Kudin, K. N.; Staroverov, V. N.; Kobayashi, R.; Normand, J.; Raghavachari, K.; Rendell, A.; Burant, J. C.; Iyengar, S. S.; Tomasi, J.; Cossi, M.;Rega, N.; Millam, N. J.; Klene, M.; Knox, J. E.; Cross, J. B.; Bakken, V.; Adamo, C.; Jaramillo, J.; Gomperts, R.; Stratmann, R. E.; Yazyev, O.; Austin, A. J.; Cammi, R.; Pomelli, C.; Ochterski, J. W.; Martin, R. L.; Morokuma, K.; Zakrzewski, V. G.; Voth, G. A.; Salvador, P.; Dannenberg, J. J.; Dapprich, S.; Daniels, A. D.; Farkas, Ö.; Foresman, J. B.; Ortiz, J. V.; Cioslowski, J.; Fox, D. J. Gaussian, Inc., Wallingford CT, 2013.

(7) Anslyn, E. V.; Dougherty, D. A. *Modern Physical Organic Chemistry*, University Science Books: Sausalito, 2004; Chapter 7.

(8) (a) Kresse, G.; Furthmüller, J. *Phys. Rev. B* **1996**, *54*, 11169. (b) Kresse, G.; Joubert, D. *Phys. Rev. B* **1999**, *59*, 1758.

(9) Blöchl, P. E. *Phys. Rev. B* **1994**, *50*, 17953.

(10) (a) Dion, M.; Rydberg, H.; Schröder, E.; Langreth, D. C.; Lundqvist, B. I. *Phys. Rev. Lett.* **2004**, *92*, 246401. (b) Jiří, K.; David, R. B.; Angelos, M. *J. Phys.: Condens. Matter* **2010**, *22*, 022201. (c) Klimeš, J.; Bowler, D. R.; Michaelides, A. *Phys. Rev. B* **2011**, *83*, 195131.

(11) Henkelman, G.; Uberuaga, B. P.; Jónsson, H. *J. Chem. Phys.* **2000**, *113*, 9901.

(12) Castiglioni, C.; Tommasini, M.; Zerbi, G. *Phil. Trans. R. Soc. Lond. A* **2004**, *362*, 2425.
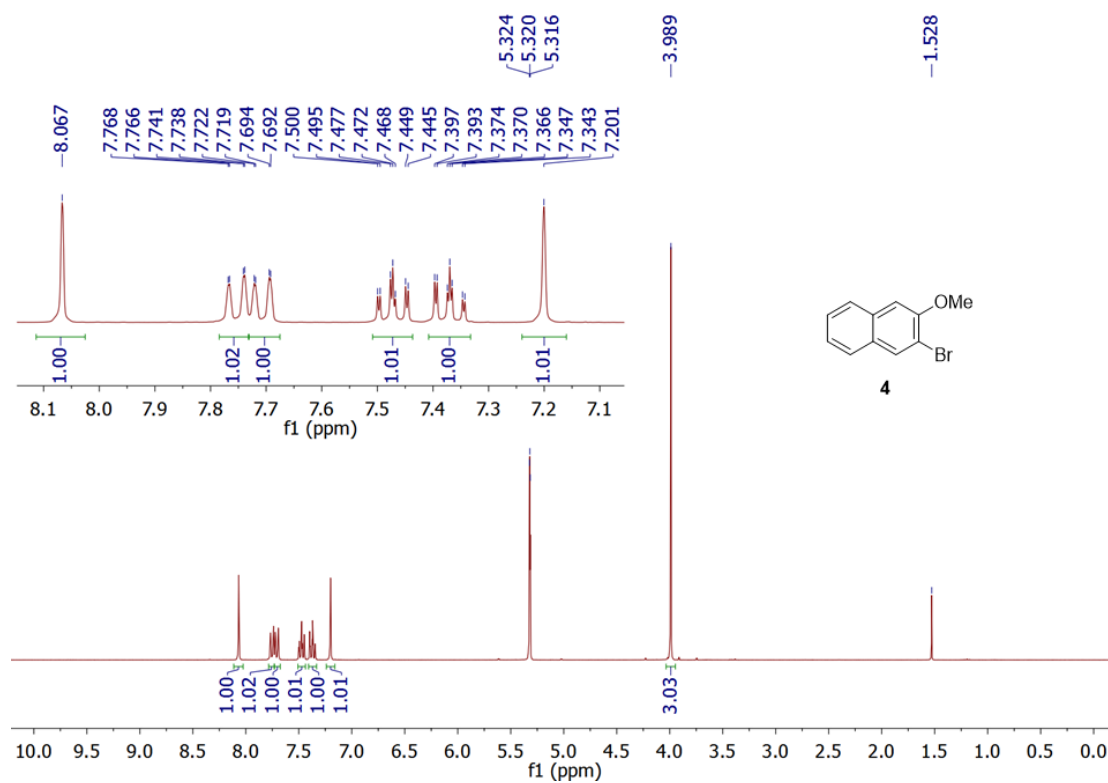
9. NMR and MS Spectra

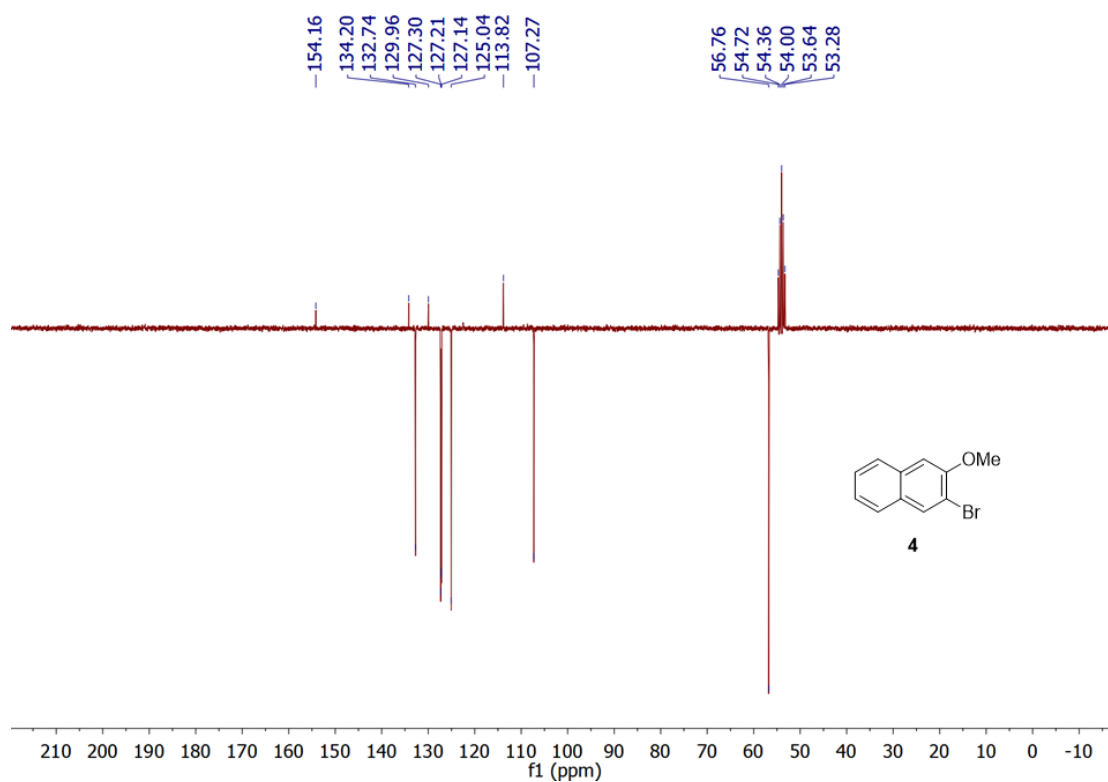**Figure S14**. ^{1}H NMR spectrum of compound **4** (300 MHz, CD$_2$Cl$_2$, 298 K).

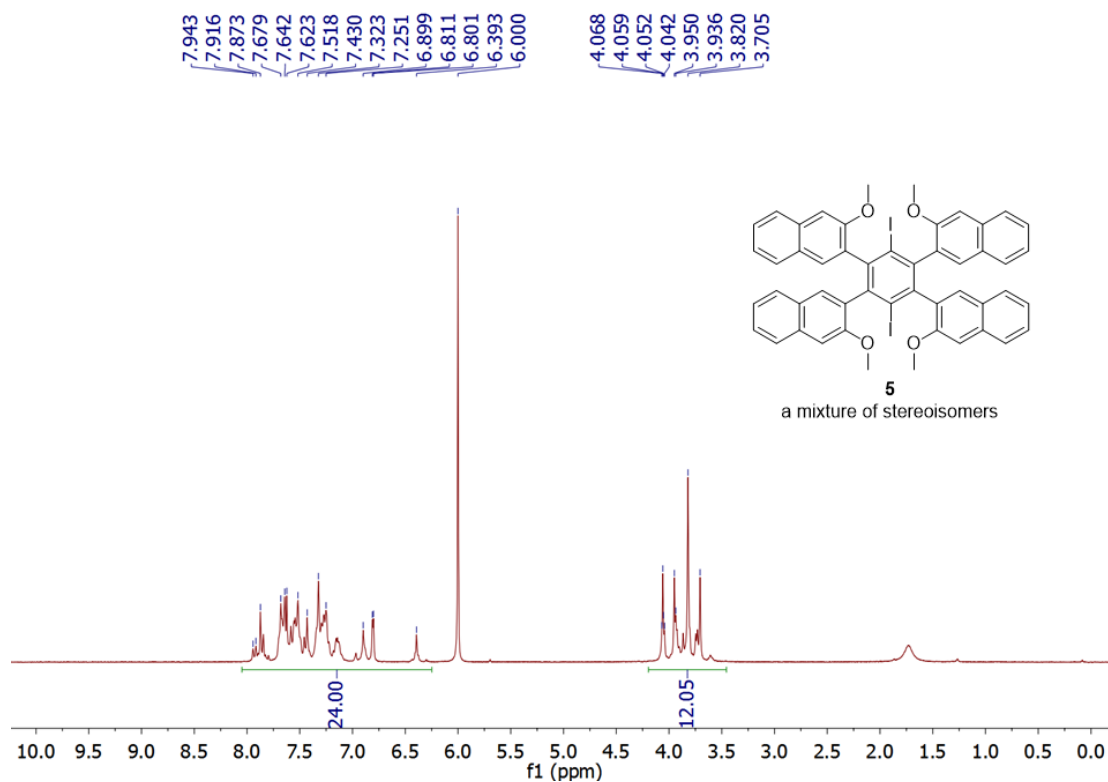**Figure S15**. ^{13}C NMR (APT) spectrum of compound **4** (75 MHz, CD$_2$Cl$_2$, 298 K).

Figure S16. ^{1}H NMR spectrum of compound **5** (300 MHz, C$_2$D$_2$Cl$_4$, 298 K).

Single Mass Analysis
Tolerance = 20.0 PPM / DBE: min = -1.5, max = 200.0
Isotope cluster parameters: Separation = 1.0 Abundance = 1.0%
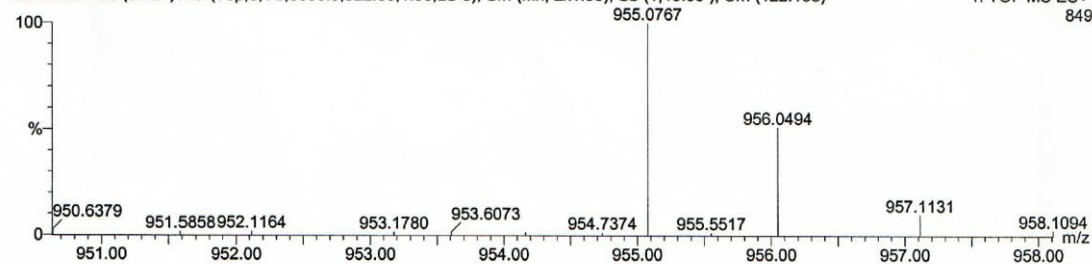
Monoisotopic Mass, Odd and Even Electron Ions
12 formula(e) evaluated with 1 results within limits (up to 50 closest results for each mass)

Wang, W181-I, Muellen
ESI26685 138 (3.421) AM (Top,8, Ar,8000.0,922.36,1.00,LS 5); Sm (Mn, 2x1.00); Sb (1,40.00); Cm (122:138)

1: TOF MS ES+
849

Minimum:				-1.5		
Maximum:		200.0	20.0	200.0		
Mass	Calc. Mass	mDa	PPM	DBE	Score	Formula
955.0767	955.0781	-1.4	-1.5	31.5	1	C50 H37 O4 127I2

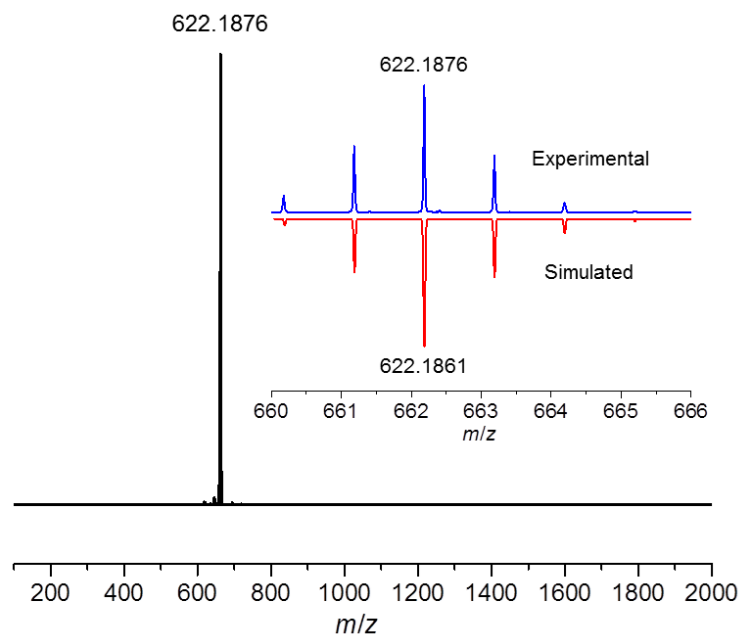**Figure S17**. High-resolution ESI-MS analysis of compound **5**.

Figure S18. High-resolution MALDI-TOF MS spectrum of compound **2**. Inset: the corresponding experimental and simulated isotopic distributions.